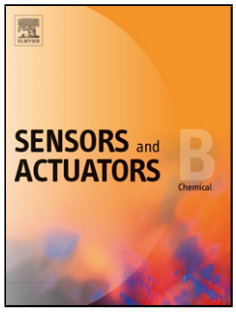

Title: A novel recyclable magnetic nanostructure for highly sensitive, selective and reversible detection of zinc ions in aqueous solutions

Author: Ghazaleh Pourfallah Xia Lou

PII: S0925-4005(16)30569-X
DOI: http://dx.doi.org/doi:10.1016/j.snb.2016.04.087
Reference: SNB 20061

To appear in: *Sensors and Actuators B*

Received date: 15-2-2016
Revised date: 11-4-2016
Accepted date: 16-4-2016

Please cite this article as: Ghazaleh Pourfallah, Xia Lou, A novel recyclable magnetic nanostructure for highly sensitive, selective and reversible detection of zinc ions in aqueous solutions, Sensors and Actuators B: Chemical http://dx.doi.org/10.1016/j.snb.2016.04.087

A novel recyclable magnetic nanostructure for highly sensitive, selective and reversible detection of zinc ions in aqueous solutions

Ghazaleh Pourfallah and Xia Lou*

Department of Chemical Engineering, Curtin University, Kent Street, Bentley, WA 6102, Australia

*Corresponding author: Email: x.lou@curtin.edu.au; Tel.: +61 9266 1682; Fax: +61 9266 2681

Abstract

The synthesis and characterisation of a novel dansylated magnetic nanostructure, namely Fe_3O_4@SiO_2-PEG-DnS, is reported here. Investigations of its fluorescent properties showed that the presence of the PEG moiety significantly enhanced the fluorescent intensity of the nanostructure when compared to both the free dansyl fluorophore and a nanostructure that contained no PEG spacer between the core and the attached dansyl group. The addition of zinc (Zn^{2+}) ions to the aqueous suspension of Fe_3O_4@SiO_2-PEG-DnS led to a 12.5-fold decrease in intensity. The quenching was selective to only Zn^{2+}. No interference was observed by other examined metal cations, including cadmium (Cd^{2+}). A very low detection limit of 6.00 nM in relation to zinc ions was demonstrated. In addition, the newly developed magnetic nanostructured chemosensor was found to be highly stable, reusable and recoverable.

Keywords: Nanosensor; magnetic chemosensor; zinc ion detection; reversible; recoverable.

1. Introduction

Developing sensors that can selectively detect zinc ions (Zn^{2+}) at low concentrations in aqueous solutions has always been an attractive topic for those who value the significance of zinc to the life sciences, mineral exploration and environmental sustainability [1,2]. Small-molecule fluorescent chemosensors are rather simple to use and have been widely used for cation detection with moderately high selectivity and sensitivity [3]. Many efforts have been focused on the development of smart fluorophores for Zn^{2+} detection, which include BODIPY [4,5], quinolone [6,7] and coumarin [8]. Despite all efforts to date, the development of a cost-effective and highly sensitive and selective chemosensor for Zn^{2+} detection remains a challenge. Magnetic core-shell nanostructures have been reported to offer recyclability/reusability of many nanomaterials, including the chemosensors, via an external magnetic field [9-11]. In many of the studies, a silica shell commonly has been used to provide stability and hydrophilicity to the magnetic nanoparticles, and to prevent possible interactions between the magnetic core and the additional functional moieties that are directly

immobilised on the silica surface [12,13]. Various silicane precursors can be covalently bonded to the silica shell, providing sites for further functionalisation via simple methods [12,14,15].

In this paper, the synthesis and characterisation of a novel magnetic core-shell nanostructure, Fe_3O_4@SiO_2-PEG-DnS, which contains a dansyl fluorophore via a poly(ethyleneglycol) (PEG) spacer, is reported. Dansyl chloride (DnCl) is a well-established fluorophore that has been widely used for the labelling and detection of amino acids, proteins and drugs [11,16,17]. It offers a large Stokes shift [18], a charge-transfer character [19] with high emission quantum yield [20] and the synthetic flexibility of the sulfonic acid group. Dansyl groups can be excited at around 325 nm, producing emission maxima typically near 510 nm [16,18]. Despite numerous attempts in regard to biological applications, the exploration of interactions between dansyl fluorophores and metal ions has been limited to small organic molecules. An early work by Schuster et al. [21] reported the complexation of Ni(II) and Cu(II) with N-dansyl-N'-ethylthiourea (DET) fluorophore, which resulted in quenching of the fluorescence. Prodi and co-workers [22] reported the synthesis of a tripodal ligand containing dansyl fluorophore, and the observation of a blue shift accompanied by an enhanced fluorescence after the addition of Zn^{2+} into the produced fluorescent molecule. Shankar et al. [23] also developed a number of dansylated chemosensors that demonstrated an effective interaction with Cu(II) by quenching of the emission intensity. PEG is hydrophilic and chemically inert. The purposes of incorporating PEG onto the surfaces of the nanoparticles include: 1) improving the stability of, and offering wettability to, the magnetic core; 2) improving the mobility of the dansyl fluorophore moiety; and 3) spatially separating the dansyl fluorophore from the magnetic core, therefore reducing the probability of core-fluorophore interactions.

A similar structure, Fe_3O_4@SiO_2-DnS, which contains no PEG spacer, also was synthesised and investigated alongside Fe_3O_4@SiO_2-PEG-DnS. The fluorescence spectra of the produced nanochemosensors and their interactions with various metal cations in aqueous solutions were further investigated. Selective interactions with Zn^{2+} have been observed. Changes in fluorescent intensity as a consequence of protonation and/or selective interaction with Zn^{2+} were investigated. The nanochemosenors, in particular the one containing PEG spacers, have shown a very low detection limit of 6 nM that is selective towards zinc ions, as well as very high reversibility and good recyclability.

2. Experimental

2.1. Materials

Sigma-Aldrich was the supplier of all chemicals used: Ferric chloride hexahydrate ($FeCl_3.6H_2O$, 99.99%), ferrous chloride tetrahydrate ($FeCl_2.4H_2O$, 99.99%), citric acid (99.5%), dansyl chloride (DnCl), tetraethoxysilane (TEOS) (99.99%), (3-glycidyloxypropyl) trimethoxylsilane (GPS) (98%), (3-aminopropyl) triethoxysilane (APS) (98%), ethanol (99.5%), O-(2-aminoethyl) polyethylene glycol ($M_w = 3000$), ammonium hydroxide (99.99%). All reagents were used, as received, without further purification. Deionised (D.I.) water was used in all experiments.

2.2. Synthesis of magnetic Fe_3O_4 nanoparticles

$FeCl_3.6H_2O$ (2.7 g, 10 mmol) and $FeCl_2.4H_2O$ (0.99 g, 5 mmol) were dissolved in 10 ml HCl solution (2 M) under vigorous stirring and nitrogen bubbling. The Fe^{2+}/Fe^{3+} solution then was added, dropwise, to 50ml sodium hydroxide solution (0.5 M) and allowed to proceed for 1 hr under mechanical stirring. After completion of the reaction, the black precipitate was isolated via an external magnet and washed sequentially four times, with 20 ml D.I. water then 20 ml ethanol each time. In order to obtain well-dispersed magnetic nanoparticles, particles were added to 2 ml citric acid solution (0.1 M) with ultrasonic treatment for 30 min. Then the mixture was maintained at room temperature for 12 hr. Finally, nanoparticles were rinsed with D.I. water (4 × 20 ml), collected from the reaction mixture by an external magnet and dispersed as a suspension in D.I. water.

2.3. Synthesis of core/shell-structured Fe_3O_4@SiO_2-APS and Fe_3O_4@SiO_2-GPS

Silanisation of the produced Fe_3O_4 nanoparticles was carried out using a previously reported method [12,24]. Fe_3O_4 nanoparticles (0.5 g, 2.16 mmol) were dispersed in a mixture of ethanol/water (30 ml, 2:1 ratio) and 1 ml ammonium hydroxide solution (25 wt%) under mechanical stirring for 1 hr. TEOS (0.5 ml, 2.25 mmol) was mixed with 5 ml ethanol, and the mixture was added, dropwise, to the prepared dispersion of Fe_3O_4 nanoparticles. The reaction then was allowed to proceed for 2 hr, under stirring at room temperature, to obtain silica-coated Fe_3O_4 nanoparticles: Fe_3O_4@SiO_2. Amino functionalisation of Fe_3O_4@SiO_2 was achieved by the dropwise addition of a mixture of APS (1.05 ml, 4.5 mmol) and 5 ml ethanol into the Fe_3O_4@SiO_2 solution, and the reaction was carried out for 2 hr under stirring. The obtained functionalised magnetic nanoparticles, Fe_3O_4@SiO_2-APS, were removed from the

reaction mixture by applying an external magnet. They were washed sequentially with 20 ml D.I. water then 20 ml ethanol, four times, and suspended in D.I. water.

Epoxy-functionalised nanoparticles, Fe_3O_4@SiO_2-GPS, were prepared by adding a solution of GPS (1.17 ml, 4.5 mmol) to the mixture, following the same procedure that was used for Fe_3O_4@SiO_2-APS. The resultant and purified Fe_3O_4@SiO_2-GPS also was suspended in D.I. water for further analyses.

2.4. Synthesis of Fe_3O_4@SiO_2-DnS

Fe_3O_4@SiO_2-APS (15 mg) was dispersed in 30 ml dry acetone. (The dry acetone was prepared through distillation of acetone after drying with calcium chloride overnight.) Triethylamine (0.5 ml, 3.58 mmol) then was added to the dispersion, and the solution was sonicated for 30 min. DnCl (45 mg, 0.166 mmol) was dissolved in 20 ml dry acetone and then added to the Fe_3O_4@SiO_2-APS dispersion. The mixture then was stirred at room temperature, in the dark, for 24 hr. The product, Fe_3O_4@SiO_2-DnS, was separated from the solution via an external magnet and washed sequentially with 20 ml each of acetone, ethanol and D.I. water in repetition for a total of four times.

2.5. Synthesis of Fe_3O_4@SiO_2-PEG-DnS

The synthesis of Fe_3O_4@SiO_2-PEG-DnS was carried out in two stages. Firstly, pegylated Fe_3O_4@SiO_2-GPS was prepared by dispersing 0.45 g of Fe_3O_4@SiO_2-GPS in 10 ml D.I. water, to which O-(2-aminoethyl) polyethylene glycol (0.135 g dissolved in 10 ml D.I. water) was added under stirring at 65ºC and further stirred for 6 hr at the same temperature. After collection via external magnet, the resultant Fe_3O_4@SiO_2-GPS-PEG was repeatedly washed with fresh D.I. water (4 × 20 ml). Then the D.I. water was sequentially substituted with acetone and dry acetone prior to the dansylation. Dansylation of the Fe_3O_4@SiO_2-GPS-PEG nanoparticles was carried out using the same procedure that was applied to Fe_3O_4@SiO_2-APS. The final product, Fe_3O_4@SiO_2-PEG-DnS, then was washed and kept as a suspension in D.I. water.

2.6. Physicochemical characterisation

Fourier transform infrared (FTIR) spectra of the products were obtained using a Thermo Scientific Nicolet iS50 for the qualitative analysis of the synthesised nanostructures. All spectra were recorded in the range of 400‑4000 cm^{-1}. X-ray diffraction (XRD) analysis was performed using a Bruker AXS diffractometer with Co Kα radiation (λ = 1.79 Å). A scan

rate of 0.015º/s was used to record the patterns in a 2θ range of 20–80º, and the accelerating voltage and current were 35 kV and 40 mA, respectively.

The produced samples also were examined using a Lambda 25 Perkin Elmer UV‑Vis Spectroscope. Scans were recorded in the wavelength range from 200 to 800 nm, with a band width of 1 nm. The size and morphology of the synthesised nanoparticles were examined using a Transmission Electron Microscope (TEM, (JEOL JSM 2011)) that was equipped with a Gatan Digital Camera. Samples were suspended in ethanol and distributed onto a carbon-coated copper grid. The TEM images were recorded at an accelerating voltage of 200 kV. For nanoparticles size measurement, thirty particles were randomly selected and the average of the thirty measurements was representatively used as the size of nanoparticles.

2.7. Fluorescence measurements

A PerkinElmer L55 fluorescence spectrometer was used, with an excitation source set at 325 nm and a scanning rate of 5 nm/min. The emission intensities of Fe_3O_4@SiO_2-DnS at 0.3 µM of the fluorophore (0.1 mg mL^{-1}) and Fe_3O_4@SiO_2-PEG-DnS at 0.3 µM of the fluorophore (0.043 mg mL^{-1}) were measured both before and after being mixed with a variety of metal ions, namely Ag^{+}, Li^{+}, Cu^{2+}, Ni^{2+}, Co^{2+}, Ca^{2+}, Cd^{2+}, Hg^{2+}, Mg^{2+}, Fe^{2+}, Mn^{2+}, Al^{3+}, Cr^{3+} and Fe^{3+}, in an aqueous solution (0.9 µM). A competition study also was carried out using aqueous solutions containing mixed metal ions.

2.8. Quantum yield measurements

Fluorescent quantum yield was examined by comparison with standard quinine sulfate dihydrate solution, using a reported method [18,25]. In brief, the stock solution (100 mg/L) was made by dissolving 5 mg quinine sulfate dihydrate in 50 ml 0.1 M H_2SO_4 solution. UV-Vis and fluorescent spectra (excited at 325 nm) were measured for the same solution. The two newly produced nanochemosensors were dispersed in aqueous solution and further diluted to 1 mg/L then subjected to the same measurements. The quantum yields of the nanochemosensors were calculated using Eq. 1:

$$\Phi = \Phi_R \frac{I\, A_R\, n^2}{I_R\, A\, {n_R}^2} \qquad (1)$$

where Φ is the quantum yield of the nanoparticles, I is the integrated intensity, A is the optical density from the UV-Vis measurement and n is the refractive index of the solvent. The subscript, R, refers to the reference fluorophore, quinine sulfate dihydrate, with a known

quantum yield [18]. In this expression, it is assumed that the sample and reference are excited at the same wavelength, so that it is not necessary to correct for the different excitation intensities of different wavelengths.

2.9. Job plot measurements

Various volumes (5, 4.5, 4, 3.5, 3, 2.5, 2, 1.5, 1 and 0.5 ml) of the produced nanochemosenors (0.3 μM, aqueous) were taken and transferred to separate vials, to which Zn^{2+} solutions (0.3 μM, aqueous) with volumes of 0, 0.5, 1, 1.5, 2, 2.5, 3, 3.5, 4 and 4.5 ml, respectively, were added. Therefore, each vial had a total volume of 5 ml solution. The fluorescent intensity of each solution was recorded and plotted against the molar fraction of Zn^{2+}.

2.10. Recovery test

The recovery of Fe_3O_4@SiO_2-PEG-DnS was carried out by following these four steps: 1) placing 5 ml suspension of Fe_3O_4@SiO_2-PEG-DnS (0.3 μM) into a vial; 2) mixing it with 5 ml Zn^{2+} solution (0.9 μM); 3) adding an equivalent amount of EDTA (5 ml, 0.9 μM) into the step 2 mixture; and 4) recovering and resuspending Fe_3O_4@SiO_2-PEG-DnS in 5 ml water by use of an external magnet followed by washing (3 × 5 ml D.I. water). The florescent intensity of the solution was recorded at each step. The procedure was repeated on the recovered nanosensor particles for another four cycles. In each cycle, three vials were used in parallel. The average of the three measurements was used for comparison. The mass of the recovered nanosensor particles also was recorded at the end of cycles 1, 3 and 5, each time using sample from one vial only.

3. Results and Discussions

3.1. Synthesis and characterisation of Fe_3O_4@SiO_2-DnS and Fe_3O_4@SiO_2-PEG-DnS

Two nanostructured magnetic chemosensors were produced using a facile synthetic pathway, displayed in Scheme 1. The synthetic pathway involved, firstly, the preparation of magnetic iron oxide (Fe_3O_4) nanoparticles that were coated with a thin shell of silica, containing either 1-aminopropyl or 3-glycidyloxypropyl functional groups, for further functionalisation. TEOS and either APS or GPS were used simultaneously in these reactions [15]. The produced functionalised silica-iron oxide nanoparticles, Fe_3O_4@SiO_2-APS, were conjugated with dansyl chloride to produce the chemosensor, Fe_3O_4@SiO_2-DnS, containing no PEG spacer (Scheme 1(a)). The GPS-functionalised silica-iron oxide nanoparticles,

Fe_3O_4@SiO_2-GPS, were first conjugated with aminated PEG, and then esterified with DnCl to produce the dansylated magnetic chemosensor containing PEG spacer, Fe_3O_4@SiO_2-PEG-DnS (Scheme 1(b)).

TEM micrographs of the nanoparticles produced at each stage of synthesis are shown in Fig. 1. The average size of the original Fe_3O_4 nanoparticles was 8 ± 3 nm. However, the size of nanoparticles increased at each subsequent stage of the chemical reactions, due to the added silica coating and organic functional groups on the surfaces of the nanoparticles. For the final products, Fe_3O_4@SiO_2-PEG-DnS and Fe_3O_4@SiO_2-DnS, the particle sizes were 33 ± 6 and 28 ± 4 nm, respectively. The presence of silica shell was well-demonstrated in all coated nanoparticles and is evident in the EDS spectrum of Fe_3O_4@SiO_2-GPS, compared with no silica present in the EDS spectrum of plain Fe_3O_4 nanoparticles.

Fig. 2(a) shows the FTIR spectra of Fe_3O_4@SiO_2-DnS and the related compounds. An absorbance at 561 cm^{-1}, which can be seen in all compounds, is associated with the stretching and vibration of Fe-O bonds. The typical vibration and stretching band of Si-O-Si at 1079 cm^{-1} can be seen in both Fe_3O_4@SiO_2-APS and Fe_3O_4@SiO_2-DnS. For the former, absorption bands at 2927 and 2861 cm^{-1} can be attributed to the C–H asymmetric and symmetric stretching vibrations of the C-H within the APS. The characteristic band at 1524 cm^{-1} is attributable to the N–H bending of primary amines. For Fe_3O_4@SiO_2-DnS, the S-O stretching vibrations at 1210 cm^{-1} and the C-N vibrations at 1150 cm^{-1} due to the presence of the dansylate group are well-demonstrated.

Fig. 2(b) displays FTIR spectra of all compounds related to the production of Fe_3O_4@SiO_2-PEG-DnS. The existence of GPS on Fe_3O_4@SiO_2 is confirmed by the presence of a new band at 903 cm^{-1}, representing the epoxy group. Absorption bands at 2927 and 2861 cm^{-1} also can be observed, attributable to the C–H stretching vibrations of GPS. After conjugation of PEG moieties onto the Fe_3O_4@SiO_2-GPS, the absorption band corresponding to the epoxy group disappears and an additional band at 3248 cm^{-1} is apparent, which supports the existence of N-H bending of the secondary amine. The stretching vibrations of S-O at 1210 cm^{-1} and C-N at 1150 cm^{-1} also can be seen in the spectra, denoting the attachment of dansyl groups.

The powder X-ray diffraction patterns of Fe_3O_4 nanoparticles and the functional nanosensors, Fe_3O_4@SiO_2-DnS and Fe_3O_4@SiO_2-PEG-DnS, are shown in Fig. 3. As can be

seen, all samples possess the characteristic diffraction peaks at (2 2 0), (3 1 1), (4 0 0), (4 2 2), (5 1 1) and (4 4 0), which are in good agreement with pure cubic Fe_3O_4 [26]. The broad peak appearing at 20–28º in the spectra for the two nanosensors corresponds to the amorphous-state silica layer and the spacer/linker attached to it, which indicates that the Fe_3O_4 magnetic cores have been successfully coated by a layer of SiO_2 and other functional groups. The XRD patterns of the nanosensors are similar to that of plain Fe_3O_4, demonstrating that the organic modification process does not induce any phase change of the Fe_3O_4 nanoparticles.

The UV-Vis spectra displayed in Fig. 4(a) further reveal the successful synthesis of Fe_3O_4@SiO_2-DnS and Fe_3O_4@SiO_2-PEG-DnS. As can be seen from the figure, free dansyl chloride exhibits absorption bands at λ_{max} = 230 and 325 nm, which correspond to π-π^* and n-π^* orbital transitions, respectively [11]. Both bands appear in Fe_3O_4@SiO_2-DnS and Fe_3O_4@SiO_2-PEG-DnS, due to the formation of dansylated species.

TGA analysis of Fe_3O_4@SiO_2-PEG-DnS, and its intermediates (Fig. 4(b)), revealed a weight loss at 35-100 °C, corresponding to the evaporation of the physically adsorbed water, and a more significant weight loss at the temperature range of 200°C to 800°C. An estimation based on these data indicates that the mole concentration of dansyl group on the surface of Fe_3O_4@SiO_2-PEG-DnS was approximately 6.66×10^{-6} mmol/mg nanoparticles. A similar analysis was performed on Fe_3O_4@SiO_2-DnS. The obtained mole concentration of dansyl group was only 3.13×10^{-6} mmol/mg nanoparticles, which is half the value demonstrated by the DnS attached to Fe_3O_4@SiO_2-PEG-DnS.

The presence of the DnS fluorophore on the surfaces of nanoparticles was further quantified by establishing a UV-Vis calibration curve at λ_{max} = 325 nm, with different molar concentrations of DnCl. The numbers of DnCl molecules attached to chemosensors were then calculated by taking the ratios of the molar concentration of DnCl obtained from the UV-calibration curve (at λ = 325 nm) to each of the initial mass concentrations of chemosensors, resulting in the numbers for Fe_3O_4@SiO_2-DnS and Fe_3O_4@SiO_2-PEG-DnS, respectively, being 3.00×10^{-6} mmol/mg and 6.92×10^{-6} mmol/mg. These results are in agreement with those obtained from TGA.

Thus, the number of DnS molecules attached to a unit mass of Fe_3O_4@SiO_2-PEG-DnS is twice that for Fe_3O_4@SiO_2-DnS. This could be attributed to the presence of the PEG spacer

in the former. Having PEG as an inert and hydrophilic spacer causes the dansylation reaction to be more facile in an aqueous environment. On the other hand, the direct attachment of DnS onto the surface of the core-shell nanostructure could be sterically hindered. For the examinations via fluorescent microscopy, discussed in the following sections, equal molar concentrations of DnS fluorophore were used for comparison.

3.2. Fluorescence studies

Fig. 5(a) shows the fluorescent responses of DnCl, Fe_3O_4@SiO_2-PEG, Fe_3O_4@SiO_2-DnS and Fe_3O_4@SiO_2-PEG-DnS in aqueous solutions. The fluorescent spectra were obtained using compounds containing the same amounts of DnS (0.3 μM), with the exception of Fe_3O_4@GPS-PEG, which contained no DnS. As can be seen from the figure, Fe_3O_4@SiO_2-PEG shows no emission, due to its lack of fluorophore. An emission at λ_{max} = 498 nm was observed for DnCl, originating from the state of charge transfer from the amine group of the dansyl to the naphthalene ring [18,27]. An enhanced fluorescence was observed for Fe_3O_4@SiO_2-DnS, which is likely to be due to intermolecular charge transfer (ICT) from the electron donor dimethylamino group to the electron withdrawal sulfonamide group, -***NH***-SO_2- (Scheme 2(a)) [27,29]. A further increase in the fluorescence intensity was observed for Fe_3O_4@SiO_2-PEG-DnS, at the maximum of 509 nm. The bonding of PEG with the dansyl group is through the more electronegative oxygen atom, thereby increasing the electron withdrawal capacity of the sulfonic ester, -***O***-SO_2-. This results in enhancement of the push-pull effect and, therefore, increased fluorescence (Scheme 2(b)). In addition, the presence of the flexible and hydrophilic PEG spacer could improve the mobility of the dansyl fluorophore in an aqueous solution, therefore further increase the fluorescence. The increased charge transfer also decreases the energy gap between the highest occupied molecular orbital (HOMO) and the lowest unoccupied molecular orbital (LUMO), leading to red-shifting of the emission wavelength [30].

Figures 5(b) and 5(c) show the fluorescent spectra of the two chemosensors, Fe_3O_4@SiO_2-DnS and Fe_3O_4@SiO_2-PEG-DnS, after the separate addition of 3.0 molar equivalent metal cations of each of Ag^+, Li^+, Zn^{2+}, Cu^{2+}, Ni^{2+}, Co^{2+}, Mg^{2+}, Mn^{2+}, Fe^{2+}, Cd^{2+}, Hg^{2+}, Ca^{2+}, Fe^{3+}, Al^{3+} and Cr^{3+} (chlorides) in D.I. water with pH = 5.6. A strong and selective quenching was demonstrated after the addition of Zn^{2+} to both sensors. The intensity values displayed in the inserts of the figures are an average of three measurements. The quenching effect was found to be much more significant in the case of Fe_3O_4@SiO_2-PEG-DnS (12.5-

fold) than for Fe_3O_4@SiO_2-DnS (2.9-fold). The dramatic reduction in florescent intensity is likely to be due to the interactions of Zn^{2+} with the dansyl moiety through complexation with the nitrogen containing electron pairs in the dimethylamine group (Scheme 2(b)), resulting in a reduction in the occurrence of this group donating electrons to the naphthalene ring. As discussed in the previous paragraph, the two newly developed nanostructures have shown increased fluorescent intensity, as a result of increased electron density caused by the injection of electrons from the electron donor dimethylamine group into the π antibonding orbital of the naphthalene ring [31,32]. The complexation between dimethylamine and Zn^{2+} would have resulted in diminishment of electron injection, leading to the observed quenching of fluorescent intensity. The quenching effect was amplified in the PEG spacer-containing sensor. This again could be due to the presence of sulfonic ester, -O-SO_2- , and the PEG-spacer. The contribution of PEG-spacer alone has been demonstrated in a following paper.

Further investigation of the pH-dependence of both the pure Fe_3O_4@SiO_2-PEG-DnS nanochemosensor and the nanosensor in the presence of added zinc cations was carried out under the same conditions. Results are shown in Fig. 6. A quenching effect is clearly presented in the pH range of 4 to 7.4, even without the presence of Zn^{2+}. This is, most likely, due to the protonation of the dimethylamino group of the chemosensor, as shown in Scheme 2(b). Protonation of dansylated fluorophores has been widely investigated, and has demonstrated a reduced charge transfer from the electron donor dimethylamino group to the electron withdrawal sulfonate group which, therefore, leads to reduced fluorescent intensity [19,21,22,33]. No quenching can be seen when the pH value is greater than 7.4. The fluorescent intensity of the nanosensor plus Zn^{2+}, in the same pH range, also is shown in Fig. 6(a). While the reduction observed in fluorescent intensity for pH values above 5.6 is attributable to the interaction of dimethylamino with Zn^{2+}, the changes in the low pH range could be due to a synergistic effect of protonation and zinc cation interaction with the nanosensor.

The complexation of Zn^{2+} with chemosensors was evident also in the absorption spectra of the chemosensors (Fig. 6(b)). As shown in the figures, the main n-π* absorption band at 325 nm in Fe_3O_4@SiO_2-PEG-DnS is diminished, presumably due to the complexation of dimethylamine with Zn^{2+} at pH = 5.6. A new band appears at ~ 255 nm, resembling the π-π* absorption band of the naphthalene ring [19]. Also shown in the figure is the influence of the pH value upon the absorption wavelength. The n-π* absorption band at

λ = 325 nm completely disappears at pH = 4. Only the π-π^* transition of the naphthalene ring is present. However, at pH = 6 and 9, there are no significant changes in the absorption spectra, indicating no modification within the naphthalene ring [19,22]. Similar results were observed for Fe_3O_4@SiO_2-DnS.

It should be noted that fluorescent quenching by Cu^{2+} and Fe^{3+} also is demonstrated in Figures 5(a) and 5(b), but by a much smaller amount. This can be attributed to the redox activity of these cations, owing to their partially filled 3d shells, which allows an electron exchange between the fluorophore and the cation via nonradiative energy transfer [12,24,34,35]. There was no significant change in the emission intensity after the addition of other metal ions, indicating a lack of interaction between those cations and the dansylated chemosensors. Moreover, both chemosensors could selectively distinguish between Zn^{2+} and Cd^{2+}, which is an extra benefit of the produced chemosensors. Cd^{2+} often demonstrates coordination properties similar to those of Zn^{2+}, due to both having a d^{10} electron configuration [36].

The fluorescent quantum yield also was determined using quinine sulfate in 0.1 M H_2SO_4 (Φ = 0.57) [18] as a reference standard. The results obtained from Equation 1 show the highest emission quantum yield for Fe_3O_4@SiO_2-PEG-DnS (Φ = 0.39), when compared with those of Fe_3O_4@SiO_2-DnS (Φ = 0.28) and free DnCl (Φ = 0.07). A Job plot was obtained to demonstrate the stoichiometry of the complexation between the nanosensors and Zn^{2+} (Fig. 7(a)). A stoichiometric ratio of 2:1 was confirmed between the nanosensors and Zn^{2+}.

To further investigate sensing properties quantitatively, fluorescence titration was performed on both nanochemosensors (0.3 μM) by varying the concentrations of Zn^{2+} (0 to 5 μM) in aqueous solution. Briefly, 2.5 ml of each of the Zn^{2+} concentrations was added to 2.5 ml of nanochemosensor solution to make a 5 ml total solution of each. The fluorescent responses of Fe_3O_4@SiO_2-DnS and Fe_3O_4@SiO_2-PEG-DnS are shown in Figures 7(b) and 7(c), respectively. A gradual decrease is seen in the fluorescent intensity of both chemosensors upon the addition of Zn^{2+}, until saturated, indicating quantitatively that Zn^{2+} is bonded to the dansyl units. A detection limit was determined by comparing the fluorescent intensities of the produced nanochemosensors with those of quenched solutions. The minimum Zn^{2+} concentration that resulted in a distinguishable intensity difference (confirmed by students using a t-test with $p < 5\%$) was taken as the detection limit. This is equivalent to

12.5 nM for Fe_3O_4@SiO_2-DnS and 6.25 nM for Fe_3O_4@SiO_2-PEG-DnS, which are both much lower values than that reported for Zn^{2+} detection (18.2 nM) in the open literature [37-39].

Competition studies also were carried out by treating the nanochemosensor with 3.0 eq. of Zn^{2+} in the presence of identical amounts of other metal ions (as listed earlier) at the same concentrations. As shown in Figures 8(a) and 8(b), most background metal ions demonstrated little or no obvious interference with the detection of Zn^{2+} ions. An apparent interference by Fe^{3+} and Cu^{2+} was shown to be due to the previously explained quenching nature of the two metal ions, indicating a more favourable interaction of the nanofluorophore with Fe^{3+} and $Cu^{2+}$and, therefore, a reduced quenching effect by the Zn^{2+}. The interference by Fe^{3+} and Cu^{2+} was less effective when the pegylated nanochemosensor was used, which is attributable to its more sensitive nature.

Reusability and regeneration is one the key factors in designing nanosensors for practical applications. The recovery of Fe_3O_4@SiO_2-PEG-DnS was examined throughout five cycles. For each cycle, the nanosensor was freed from the Zn^{2+} ions by treating each solution with EDTA in base (pH = 8) conditions. The fluorescent intensity was examined and a 98.3% recovery was observed after five cycles (Fig. 8(c)). The mass recoverability also was examined, and was found to be 94.0%, 88.8% and 76.4% after the 1st, 3rd and 5th cycles, respectively. The results demonstrated the excellent stability of the nanochemosensor and its recyclability for practical applications.

4. Conclusions

In summary, this communication reports the successful fabrication and characterisation of a novel magnetic nanochemosensor, namely Fe_3O_4@SiO_2-PEG-DnS, and includes the investigation results in regard to its sensitivity, selectivity, detection limit and pH dependence, as well as its stability and reusability in relation to a series of metal ions. A strong and selective fluorescent quenching was obtained in regard to Zn^{2+} in aqueous solutions. The contributions from both zinc-complexation and/or protonation of the dimethylamine group in the dansyl fluorophore have been hypothesised, both of which are pH dependent. In comparison with Fe_3O_4@SiO_2-DnS, which contains no PEG spacer, Fe_3O_4@SiO_2-PEG-DnS showed a significantly improved sensitivity and selectivity towards zinc ions (Zn^{2+}). Fe_3O_4@SiO_2-PEG-DnS also displayed a noticeably higher value for the

quantum yield (0.39) than that of the non-spacer chemosensor (Φ = 0.28), and a very sensitive detection limit of 6.00 nM in regard to zinc ions, which is lower than the lowest reported value of 18.2 nM. In addition, the nanochemosensors displayed very good selectivity when in competition with other cations, except for Cu^{2+} and Fe^{3+}. Furthermore, the novel Fe_3O_4@SiO_2-PEG-DnS nanosensor has proven to be very stable and highly recoverable. Both chemosensors selectively distinguished Zn^{2+} from Cd^{2+}, which is an additional benefit.

References

[1] P. Jiang, Z. Guo, Fluorescent detection of zinc in biological systems: recent development on the design of chemosensors and biosensors, Coord. Chem. Rev. 248 (2004) 205-229.

[2] Z. Xu, J. Yoon, D.R. Spring, Fluorescent chemosensors for Zn^{2+}, Chem. Soc. Rev. 39 (2010) 1996-2006.

[3] J. Wu, W. Liu, J. Ge, H. Zhang, P. Wang, New sensing mechanisms for design of fluorescent chemosensors emerging in recent years, Chem. Soc. Rev. 40 (2011) 3483-3495.

[4] J. Cao, C. Zhao, X. Wang, Y. Zhang, W. Zhu, Target-triggered deprotonation of 6-hydroxyindole-based BODIPY: specially switch on NIR fluorescence upon selectively binding to Zn^{2+}, Chem. Commun. 48 (2012) 9897-9899.

[5] Y. Wu, X. Peng, B. Guo, J. Fan, Z. Zhang, J. Wang, et al., Boron dipyrromethene fluorophore based fluorescence sensor for the selective imaging of Zn(II) in living cells, Org. Biomol. Chem. 3 (2005) 1387-1392.

[6] I. Ravikumar, P. Ghosh, Zinc(II) and PPi selective fluorescence OFF–ON–OFF functionality of a chemosensor in physiological conditions, Inorg. Chem. 50 (2011) 4229-4231.

[7] X. Zhou, B. Yu, Y. Guo, X. Tang, H. Zhang, W. Liu, Both visual and fluorescent sensor for Zn^{2+} based on quinoline platform, Inorg. Chem. 49 (2010) 4002-4007.

[8] Z. Xu, X. Liu, J. Pan, D.R. Spring, Coumarin-derived transformable fluorescent sensor for Zn^{2+}, Chem. Commun. 48 (2012) 4764-4766.

[9] Y. Wang, X. Peng, J. Shi, X. Tang, J. Jiang, W. Liu, Highly selective fluorescent chemosensor for Zn^{2+} derived from inorganic-organic hybrid magnetic core/shell $Fe_3O_4@SiO_2$ nanoparticles, Nanoscale Res. Lett. 7 (2012) 1-13.

[10] M. Park, S. Seo, I.S. Lee, J.H. Jung, Ultraefficient separation and sensing of mercury and methylmercury ions in drinking water by using aminonaphthalimide-functionalized $Fe_3O_4@SiO_2$ core/shell magnetic nanoparticles, Chem. Commun. 46 (2010) 4478-4480.

[11] G. Liu, H. Wu, H. Zheng, L. Tang, H. Hu, H. Yang, et al., Synthesis and applications of fluorescent-magnetic-bifunctional dansylated $Fe_3O_4@SiO_2$ nanoparticles, J. Mater. Sci. 46 (2011) 5959-5968.

[12] X. Feng, S. Zhang, X. Lou, Controlling silica coating thickness on TiO_2 nanoparticles for effective photodynamic therapy, Colloids Surf., B 107 (2013) 220-226.

[13] A.H. Lu, E.e.L. Salabas, F. Schüth, Magnetic nanoparticles: synthesis, protection, functionalization, and application, Angew. Chem. Int. Ed. 46 (2007) 1222-1244.

[14] L. Tian, X. Lou, Z.Q. Pan, Q.M. Huang, H. Zhou, Synthesis, characterisation and catalase-like activity of silica-coated magnetite nanoparticles modified by a Schiff base Mn complex, Micro Nano Lett. 8 (2013) 159-162.

[15] X. Lou, T. Schumacher, H. Yang, A. Ding, Synthesis and characterisation of silica–polymer hybrid core–shell and hollow spheres for drug delivery applications, J. Controlled Release 152 (2011) e65-e67.

[16] H. Wu, P. Zhou, J. Wang, L. Zhao, C. Duan, Dansyl-based fluorescent chemosensors for selective responses of Cr(III), New J. Chem. 33 (2009) 653-658.

[17] G.G. Talanova, N.S. Elkarim, V.S. Talanov, R.A. Bartsch, A calixarene-based fluorogenic reagent for selective mercury(II) recognition, Anal. Chem. 71 (1999) 3106-3109.

[18] J.R. Lakowicz, B.R. Masters, Principles of fluorescence spectroscopy, J. Biomed. Opt. 13 (2008) 9901.

[19] M. Montalti, L. Prodi, N. Zaccheroni, G. Falini, Solvent-induced modulation of collective photophysical processes in fluorescent silica nanoparticles, JACS 124 (2002) 13540-13546.

[20] Q.Y. Chen, C.F. Chen, A new Hg^{2+}-selective fluorescent sensor based on a dansyl amide-armed calix [4]-aza-crown, Tetrahedron Lett. 46 (2005) 165-168.

[21] M. Schuster, M. Šandor, N-Dansyl-N′-ethylthiourea for the fluorometric detection of heavy metal ions, Fresenius J. Anal. Chem. 356 (1996) 326-330.

[22] L. Prodi, F. Bolletta, M. Montalti, N. Zaccheroni, Searching for new luminescent sensors: synthesis and photophysical properties of a tripodal ligand incorporating the dansyl chromophore and of its metal complexes, Eur. J. Inorg. Chem. 1999 (1999) 455-460.

[23] B.H. Shankar, D. Ramaiah, Dansyl-Naphthalimide Dyads As Molecular Probes: Effect of Spacer Group on Metal Ion Binding Properties, J. Phys. Chem. B 115 (2011) 13292-13299.

[24] X. Feng, S. Zhang, H. Wu, X. Lou, A novel folic acid-conjugated TiO_2–SiO_2 photosensitizer for cancer targeting in photodynamic therapy, Colloids Surf., B 125 (2015) 197-205.

[25] G.A. Crosby, J.N. Demas, Measurement of photoluminescence quantum yields. Review, J. Phys. Chem. 75 (1971) 991-1024.

[26] J. Feng, J. Mao, X. Wen, M. Tu, Ultrasonic-assisted in situ synthesis and characterization of superparamagnetic Fe_3O_4 nanoparticles, J. Alloys Compd. 509 (2011) 9093-9097.

[27] L. Prodi, F. Bolletta, M. Montalti, N. Zaccheroni, Luminescent chemosensors for transition metal ions, Coord. Chem. Rev. 205 (2000) 59-83.

[28] B.P. Joshi, C.R. Lohani, K.-H. Lee, A highly sensitive and selective detection of Hg(II) in 100% aqueous solution with fluorescent labeled dimerized Cys residues, Org. Biomol. Chem. 8 (2010) 3220-3226.

[29] V. Tharmaraj, K. Pitchumani, An acyclic, dansyl based colorimetric and fluorescent chemosensor for Hg(II) via twisted intramolecular charge transfer (TICT), Anal. Chim. Acta 751 (2012) 171-175.

[30] H. Maeda, T. Maeda, K. Mizuno, Absorption and fluorescence spectroscopic properties of 1-and 1, 4-silyl-substituted naphthalene derivatives, Molecules 17 (2012) 5108-5125.

[31] G. Weber, F.J. Farris, Synthesis and spectral properties of a hydrophobic fluorescent probe: 6-propionyl-2-(dimethylamino) naphthalene, Biochemistry 18 (1979) 3075-3078.

[32] W. Schmidt, Optical spectroscopy in chemistry and life sciences, Wiley-VCH, 2005.

[33] T. Koike, T. Watanabe, S. Aoki, E. Kimura, M. Shiro, A novel biomimetic zinc(II)-fluorophore, dansylamidoethyl-pendant macrocyclic tetraamine 1, 4, 7, 10-tetraazacyclododecane (cyclen), JACS 118 (1996) 12696-12703.

[34] L. Fabbrizzi, M. Licchelli, P. Pallavicini, D. Sacchi, A. Taglietti, Sensing of transition metals through fluorescence quenching or enhancement. A review, Analyst 121 (1996) 1763-1768.

[35] B. Valeur, I. Leray, Design principles of fluorescent molecular sensors for cation recognition, Coord. Chem. Rev. 205 (2000) 3-40.

[36] K. Hanaoka, K. Kikuchi, H. Kojima, Y. Urano, T. Nagano, Development of a zinc ion-selective luminescent lanthanide chemosensor for biological applications, JACS 126 (2004) 12470-12476.

[37] G.J. Park, Y.J. Na, H.Y. Jo, S.A. Lee, A.R. Kim, I. Noh, et al., A single chemosensor for multiple analytes: fluorogenic detection of Zn^{2+} and OAc^{-} ions in aqueous solution, and an application to bioimaging, New J. Chem. 38 (2014) 2587-2594.

[38] Y. Ma, H. Chen, F. Wang, S. Kambam, Y. Wang, C. Mao, et al., A highly sensitive and selective ratiometric fluorescent sensor for Zn^{2+} ion based on ICT and FRET, Dyes Pigm. 102 (2014) 301-307.

[39] E.J. Song, H. Kim, I.H. Hwang, K.B. Kim, A.R. Kim, I. Noh, et al., A single fluorescent chemosensor for multiple target ions: recognition of Zn^{2+} in 100% aqueous solution and F^{-} in organic solvent, Sens. Actuators, B 195 (2014) 36-43.

Figure Captions

Fig. 1. (a) TEM images of magnetic nanoparticles, (b) EDS spectrum of Fe_3O_4 and Fe_3O_4@SiO_2-GPS. Cu and C in EDS spectrum are from the copper grid and carbon coating on the copper, respectively

Fig. 2. FTIR spectra of all nanoparticles related to (a) Fe_3O_4@SiO_2-DnS and (b) Fe_3O_4@SiO_2-PEG-DnS

Fig. 3. XRD patterns of Fe_3O_4, Fe_3O_4@SiO_2-DnS and Fe_3O_4@SiO_2-PEG-DnS

Fig. 4. (a) UV-Vis spectra of DnCl, Fe_3O_4@SiO_2-DnS and Fe_3O_4@SiO_2-PEG-DnS and (b) thermal curves showing thermogravimetric loss of Fe_3O_4@SiO_2-PEG-DnS at various temperature ranges

Fig. 5. Fluorescent emission spectra of (a) DnCl, Fe_3O_4@SiO_2-PEG, Fe_3O_4@SiO_2-DnS and Fe_3O_4@SiO_2-PEG-DnS, and both (b) Fe_3O_4@SiO_2-DnS and (c) Fe_3O_4@SiO_2-PEG-DnS towards different metal cations

Fig. 6. (a) Fluorescent intensity of Fe_3O_4@SiO_2-PEG-DnS at different pH values and (b) absorption spectra of Fe_3O_4@SiO_2-PEG-DnSunder various conditions. Both are contrasted with results upon the addition of 3.0 equiv. of Zn^{2+}

Fig. 7. (a) The Job plot of Fe_3O_4@SiO_2-DnS and Fe_3O_4@SiO_2-PEG-DnS, and fluorescence spectra of (b) Fe_3O_4@SiO_2-DnS and (c) Fe_3O_4@SiO_2-PEG-DnS, all upon the addition of Zn^{2+} (0-5 μM) in aqueous solution. Sensor concentration is 0.3 μM

Fig. 8. Fluorescent emission changes of (a) Fe_3O_4@SiO_2-DnS and (b) Fe_3O_4@SiO_2-PEG-DnS at 0.3 μM upon the addition of various metal cations (3.0 equivalents), and (c) the recoverability of Fe_3O_4@SiO_2-PEG-DnS with Zn^{2+}

Fig. 1.

(a)

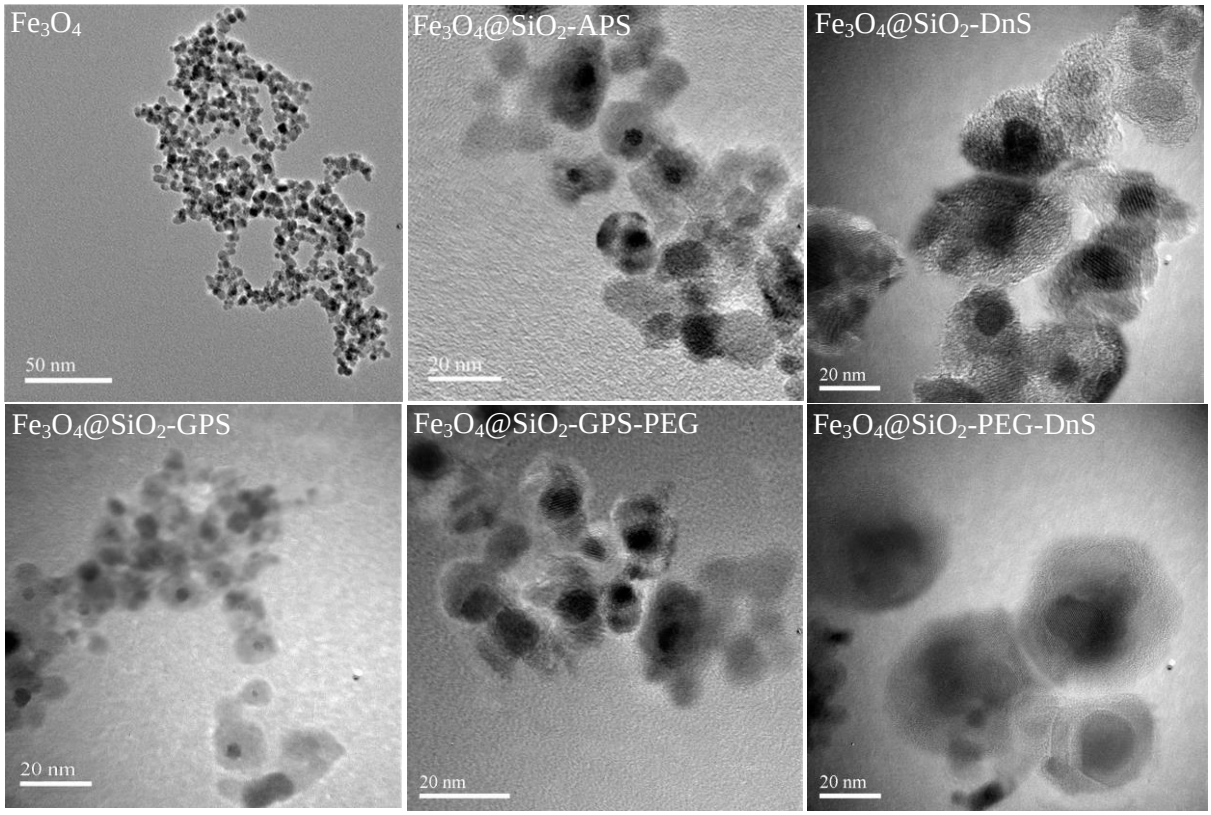

(b)

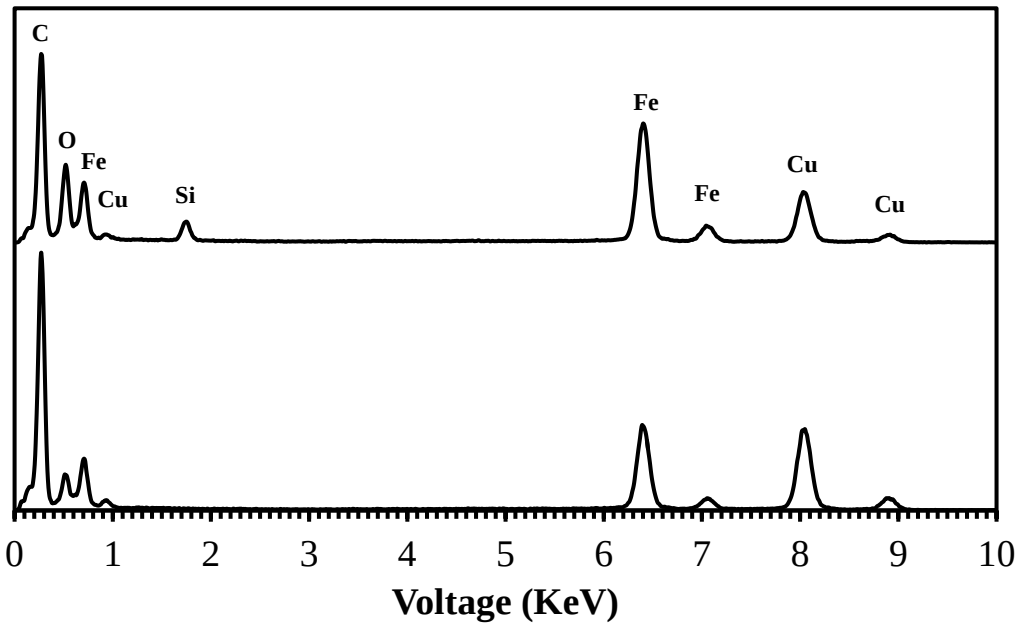

Fig. 2.

(a)

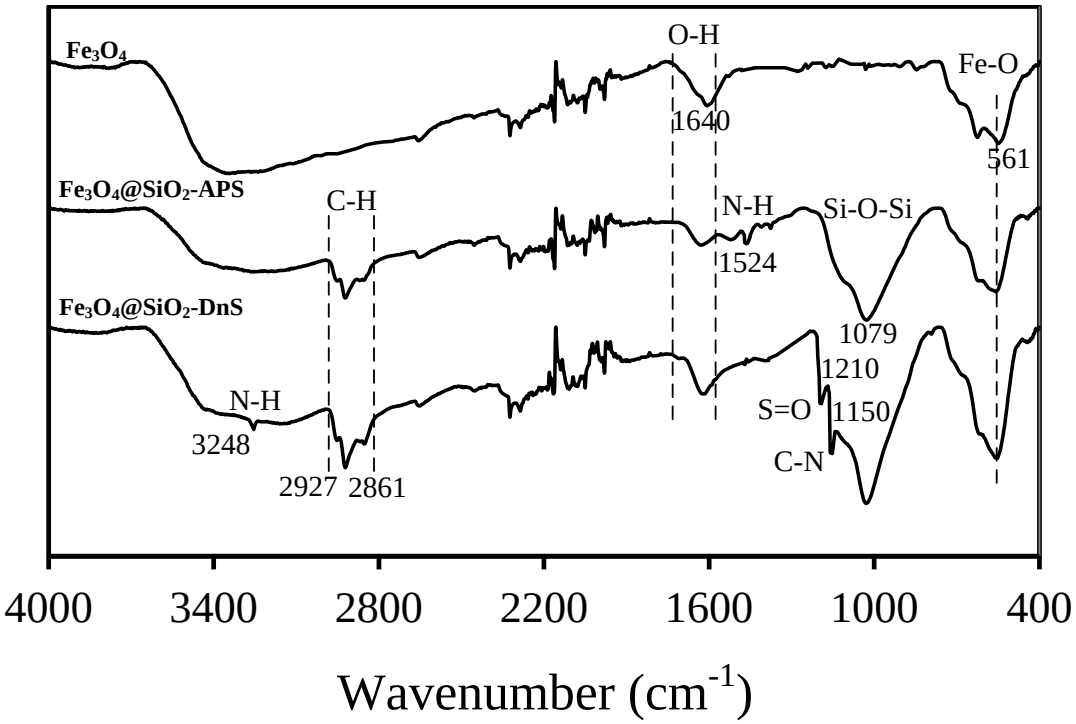

(b)

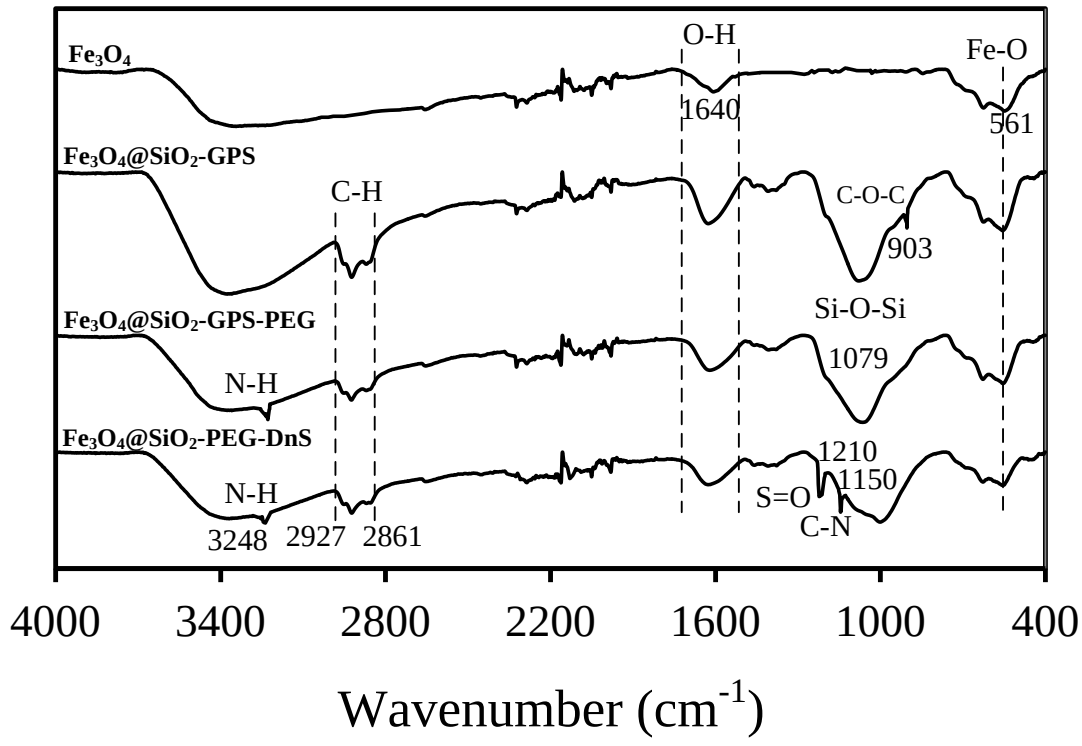

Fig. 3.

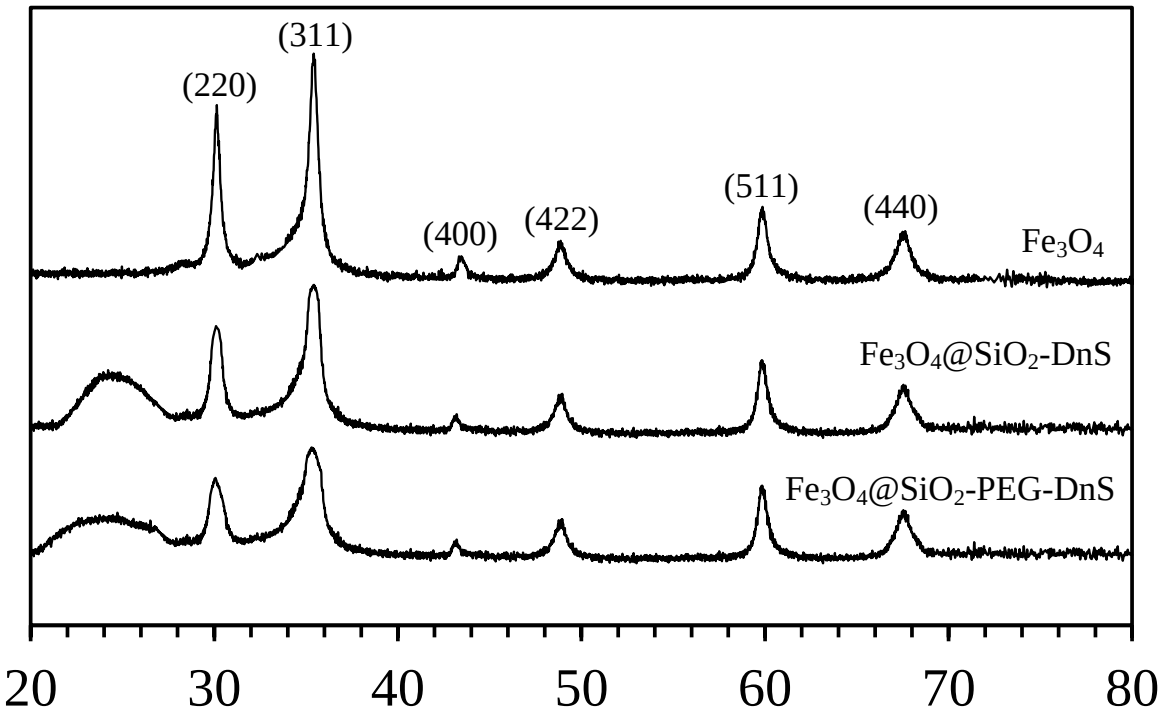

Fig. 4.

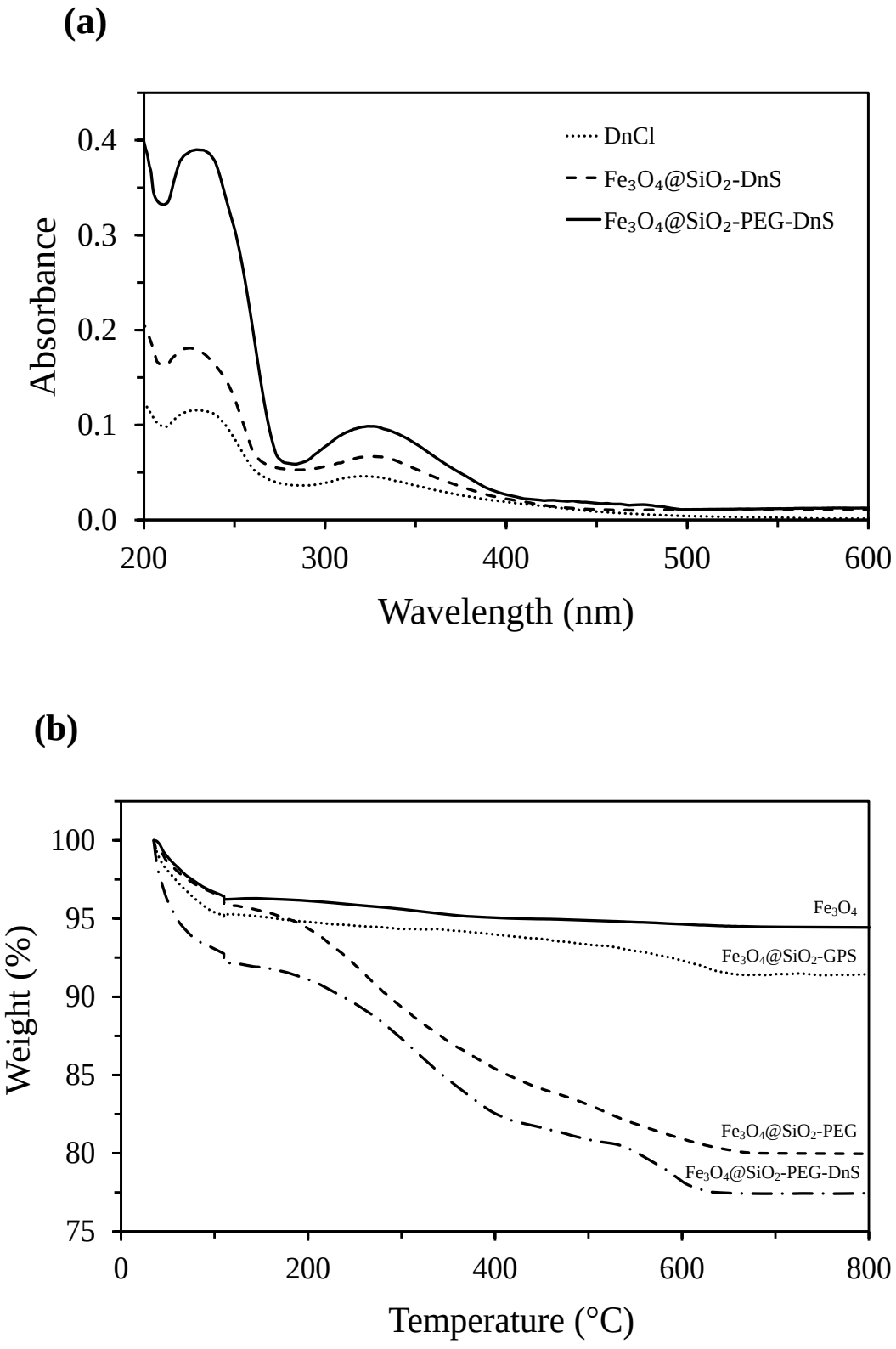

Fig. 5.

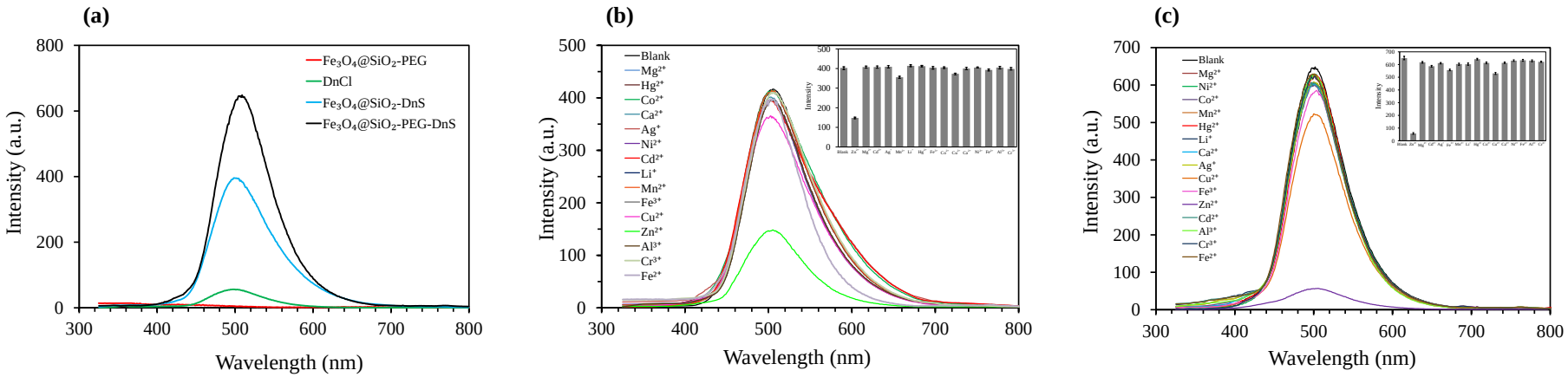

Fig. 6.

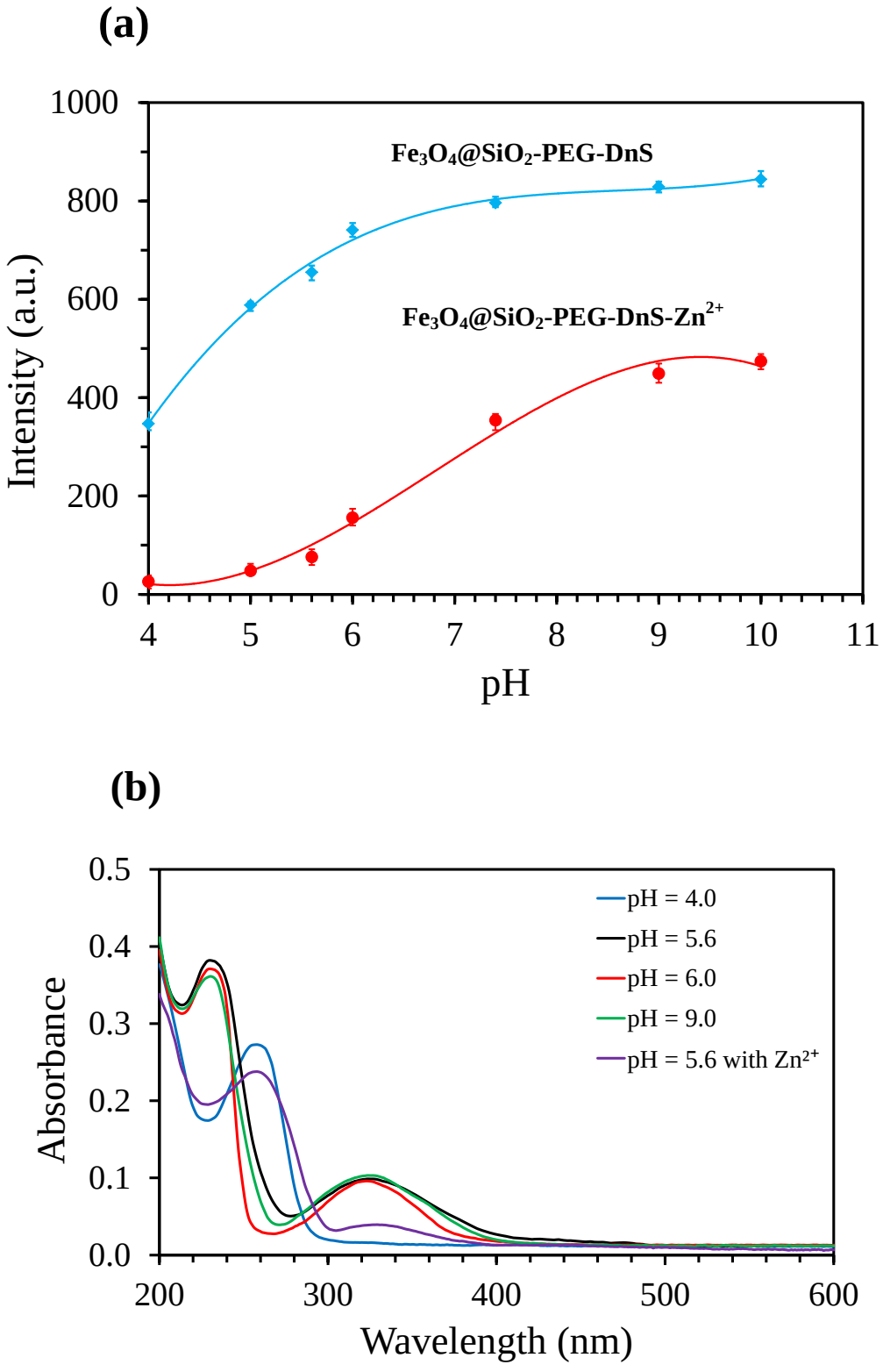

Fig. 7.

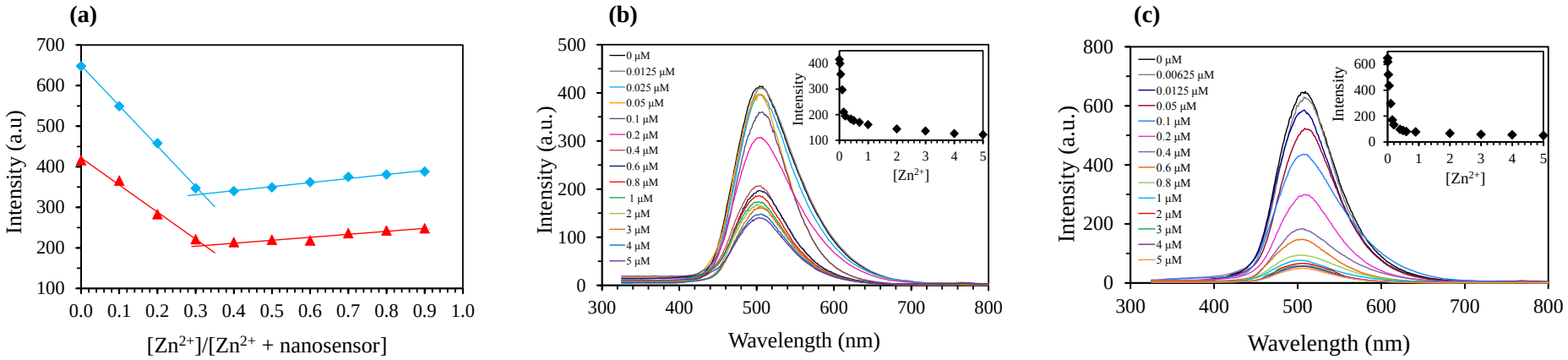

Fig. 8.

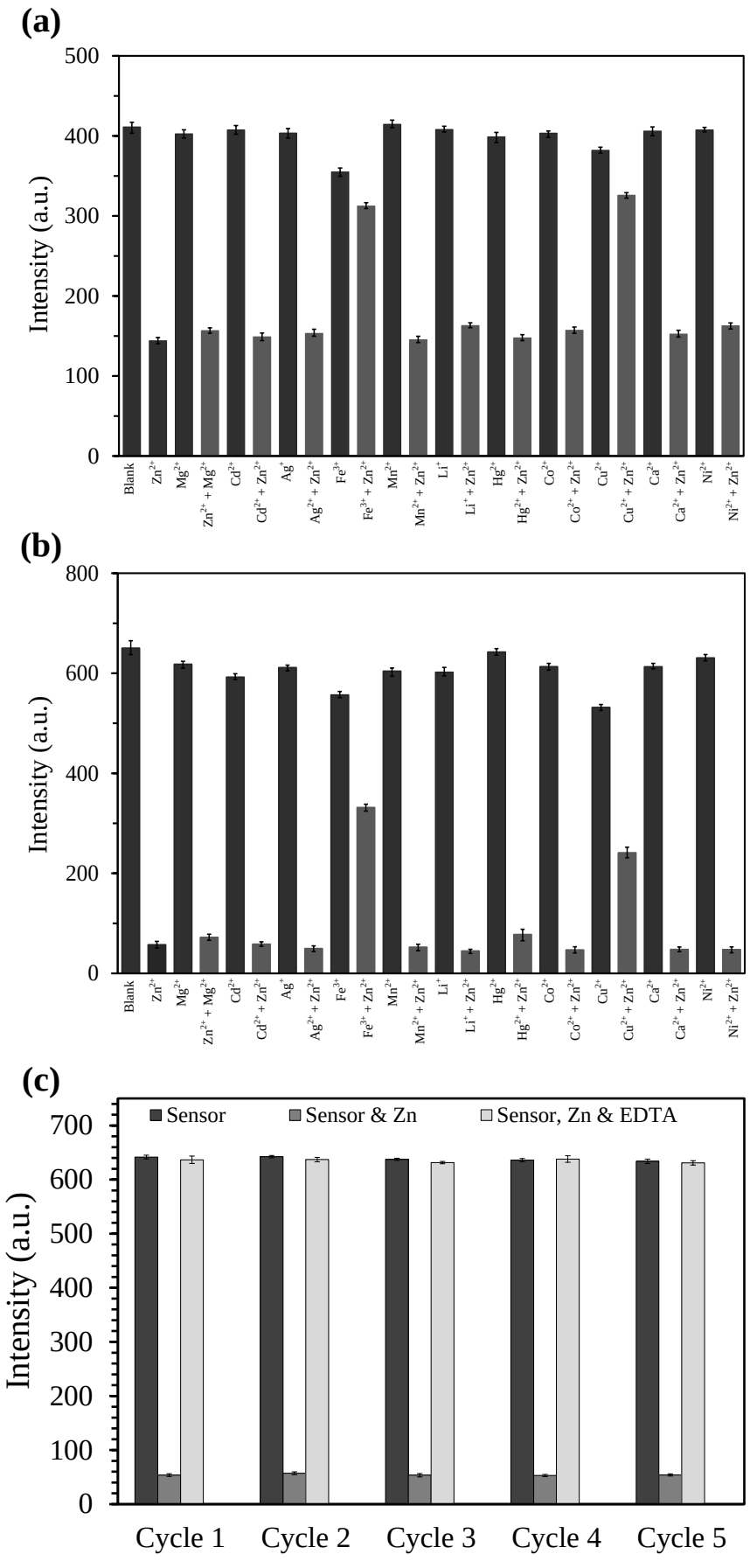

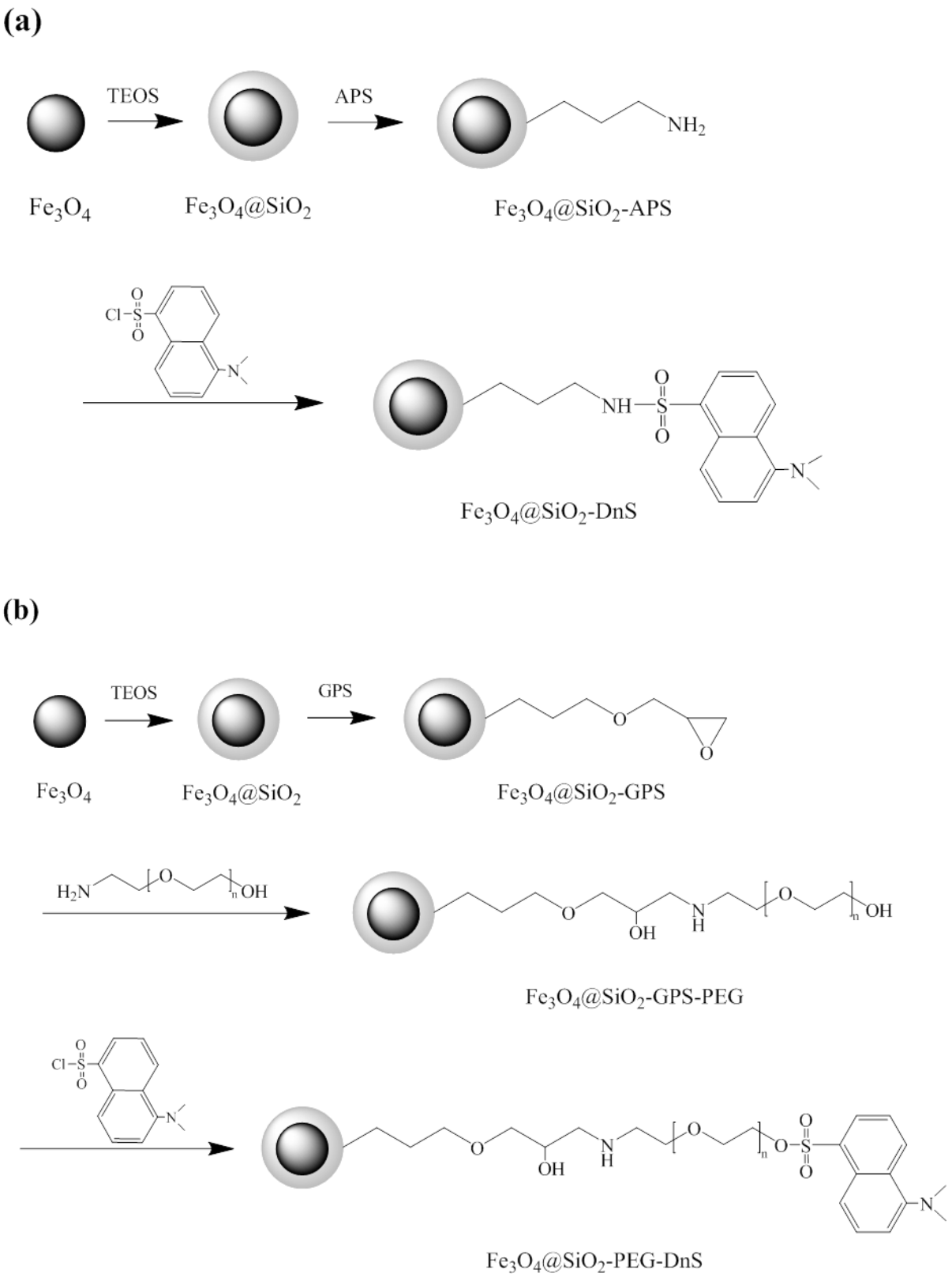

Scheme 1. Synthetic pathways for the dansylated magnetic nanochemosensors

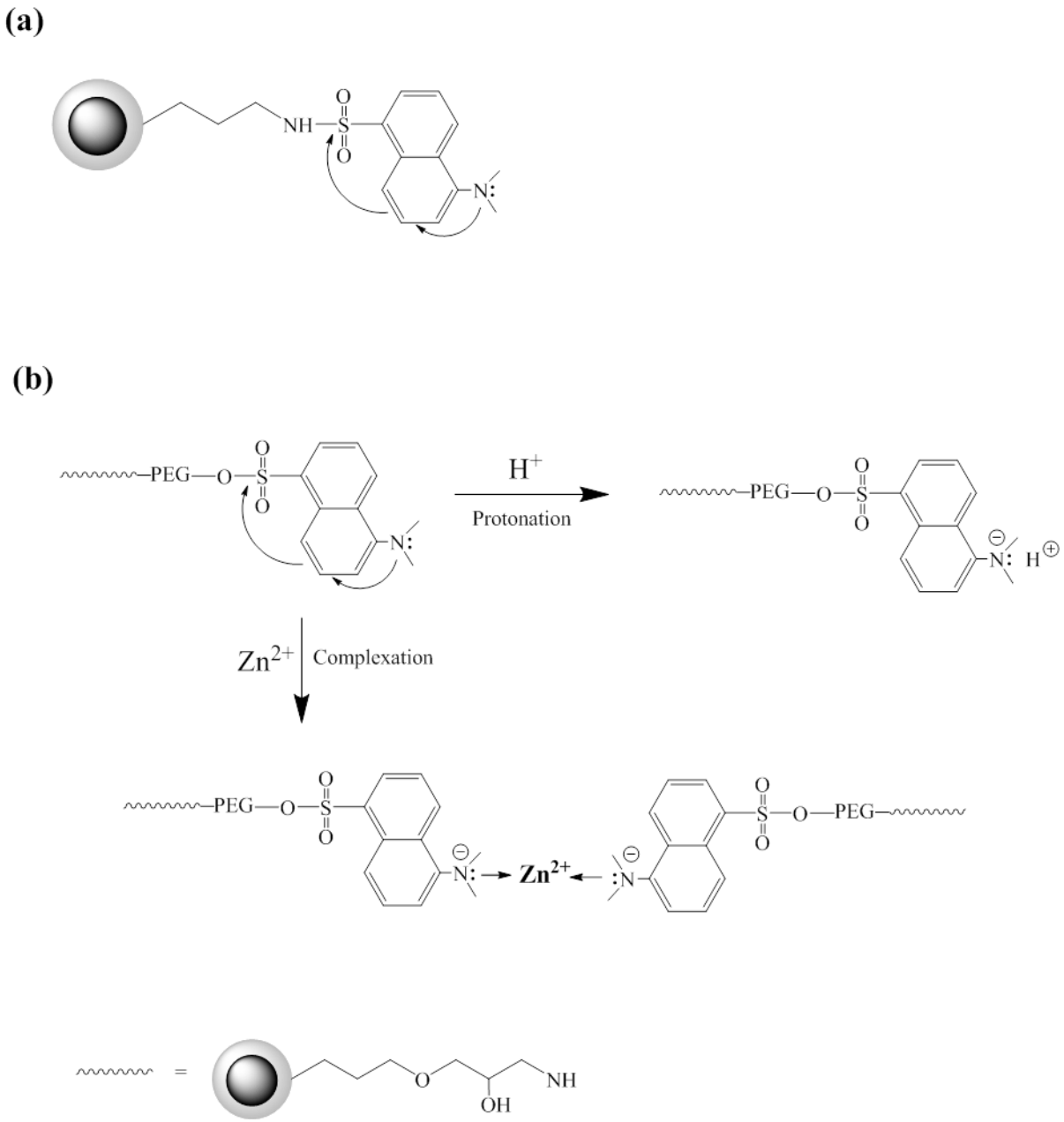

Scheme 2. Illustration of enhanced push-pull effect in (a) Fe_3O_4@SiO_2-DnS and (b) Fe_3O_4@SiO_2-PEG-DnS, showing the hypothesised protonation and Zn^{2+} complexation mechanisms